Experimental equation of state in pp and p$\bar{\text{p}}$ collisions and phase transition to quark gluon plasma

Renato Campanini[a,b,*], Gianluca Ferri[a]

[a] *Università di Bologna, Dipartimento di Fisica, viale C. Berti Pichat 6/2, I-40127, Bologna, Italy*
[b] *INFN, Sezione di Bologna, viale C. Berti Pichat 6/2, I-40127, Bologna, Italy*

Abstract

We deduce approximate equations of state from experimental measurements in pp and p$\bar{\text{p}}$ collisions. Thermodynamic quantities are estimated combining the measure of average transverse momentum $\langle p_T \rangle$ vs pseudorapidity density $\frac{dN_{ch}}{d\eta}$ with the estimation of the interaction region size from measures of Bose Einstein correlation, or from a theoretical model which relates $\frac{dN_{ch}}{d\eta}$ to the impact parameter. The results are very similar to theory predictions in case of crossover from hadron gas to quark gluon plasma. According to our analysis, the possible crossover should start at $\frac{dN_{ch}}{d\eta} \simeq 6$ and end at $\frac{dN_{ch}}{d\eta} \simeq 24$.

Keywords:
quark gluon plasma, average transverse momentum vs pseudorapidity density, equation of state, Bose Einstein correlation, hadron gas, sound velocity

*Corresponding Author: Tel. +39 051 2095078, Fax +39 051 2095047, Mobile +39 3485925020

Email addresses: Renato.Campanini@bo.infn.it (Renato Campanini), g.ferri@unibo.it (Gianluca Ferri)

1. Introduction

Some of the most important questions about the transition to the quark gluon plasma (QGP), a new state of matter with partonic degrees freedom, are not yet fully answered. Among them the location of phase boundaries between hadronic gas and the QGP. The results of lattice QCD simulations concerning the order of phase transition depend strongly on the number of quark flavors and on the quark masses. For vanishing baryon chemical potential $\mu_b = 0$, the nature of transition can be a genuine phase transition (first order or continuous), or just a rapid change (crossover) over a small temperature range [1]. Estimates of energy densities which can be achieved in ultra-relativistic pp or $p\bar{p}$ collisions with high multiplicities suggest values sufficiently high for experimental formation of the QGP [2].

However it may be that, unlike what happens in heavy ion interactions, in pp and $p\bar{p}$ the central blob of created matter never thermalizes [3], although there are different opinions [2, 4–7] which predict that thermodynamics concepts may be applied in pp or $p\bar{p}$ high multiplicity events.

Probes of equation of state are among possible signatures of phase transition or crossover. The basic idea behind this class of signatures is the identification of modifications in the dependence of energy density ϵ, pressure P and entropy density σ of hadronic matter on temperature T. One wants to search for a rapid rise in the effective number of degrees of freedom, as expressed by the ratio ϵ/T^4 or σ/T^3, over a small temperature range. One can expect a step-like rise as predicted by lattice simulations (Fig. 1), more or less steep depending from the presence of transition or crossover, and from the order of the transition in the former case. Finite volume effects may

cause important consequences for ϵ/T^4 and σ/T^3: the latent heat and the jump in the entropy density are considerably reduced for small systems [8]. Besides that, the critical temperature may shift to higher temperatures and the width of the transition may broaden for smaller volumes and there may be a smoothening of singularities due to the finite size of the system [8–10].

In 1982 it has been suggested by Van Hove [12] that an anomalous behavior of average transverse momentum $\langle p_T \rangle$ as function of the multiplicity could be a signal for the occurrence of a phase transition in hadronic matter. His conjecture is based on the idea that the $\langle p_T \rangle$ distribution of secondaries reflects the temperature of the system and its evolution in the transverse direction, while the multiplicity per unit rapidity provides a measure of entropy [13, 14]. In a recent paper [15] one of us showed that from 22 to 7000 GeV in 21 $\langle p_T \rangle$ vs pseudorapidity density $\frac{dN_{ch}}{d\eta}$ curves there is a slope change at $\frac{dN_{ch}}{d\eta} = 5.5 \pm 1.2$. Signals related to these slope changes may indicate transition to a new mechanism of particle production. Many years ago, in [16], we pointed out that pp at ISR and p$\bar{\text{p}}$ data at CERN collider showed a kind of jump at $\frac{dN_{ch}}{d\eta} = 6$ and that it had to be investigated as a possible phase transition signal [17]. In 2002, Alexopoulos et al. [18] assumed that the system produced in p$\bar{\text{p}}$ at $\sqrt{s} = 1800$ GeV for $\frac{dN_{ch}}{d\eta} > 6.75$ was above the deconfinement transition to explain their experimental results.

In present article, taking into account experimental results in pp and p$\bar{\text{p}}$ at high energies [19–32], we show how measured physical quantities satisfy relations which, given proper approximations and correspondences, can give a representation of the equations of state (EOS) that describe the created system in the central region in pseudorapidity in high energy pp and p$\bar{\text{p}}$

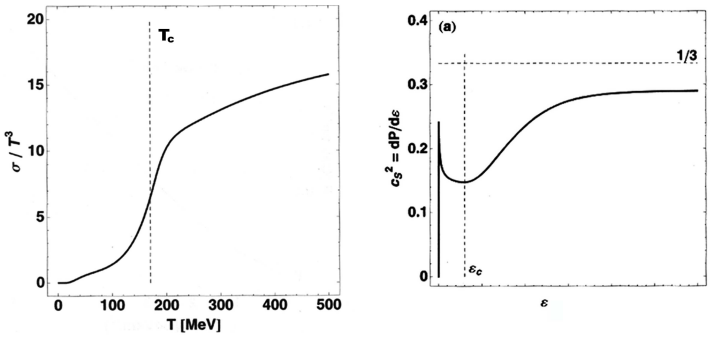

(a)

(b)

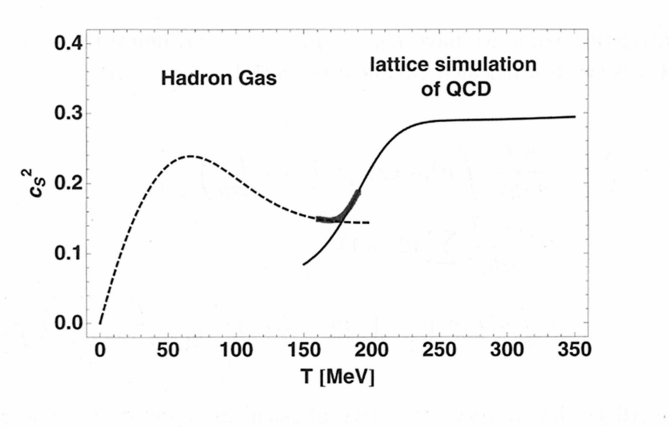

(c)

Figure 1: Results of the lattice simulations of QCD for $T > T_c$ (critical temperature) and from ideal hadron-gas model for $T < T_c$.

1a: entropy density σ scaled by T^3 calculated in the hadron-gas model and by lattice simulations of QCD shown as function of temperature. The vertical line indicates the critical temperature.

1b: sound velocity c_s^2 shown as function of the energy density ϵ.

1c: temperature dependence of the square of the sound velocity at zero baryon density as function of T. In this case the critical temperature T is equal to 170 MeV.

From [11].

collisions. Starting from $\langle p_T \rangle$ vs $\frac{dN_{ch}}{d\eta}$ experimental results together with the estimation of the size S of the interaction area, which is obtained from the measurements of the radii of emission in function of multiplicities [23–26], or from a model which relates multiplicity to impact parameter [33], we obtain relations among $\langle p_T \rangle$ and particle density σ_S, which seem to resemble EOS curves predicted for hadronic matter with crossover to QGP. The $\langle p_T \rangle$ and S vs $\frac{dN_{ch}}{d\eta}$ relations contain the relevant information, which translates in $\langle p_T \rangle$ vs σ_S correlations.

According to our knowledge, this is the first attempt to obtain an estimation of the complete EOS for hadronic matter using experimental data only.

2. Methods

The experimental results and the approximations made in this work are the following.

2.1. $\langle p_T \rangle$ *vs* $\frac{dN_{ch}}{d\eta}$

As we mentioned before, $\langle p_T \rangle$ vs $\frac{dN_{ch}}{d\eta}$ correlation at about $\frac{dN_{ch}}{d\eta} = 6$ shows a slope change in all the experiments. In Van Hove scheme $\langle p_T \rangle$ reflects temperature and the system evolution. On the other hand, the biggest part of emitted particles is constituted by pions and the pion $\langle p_T \rangle$ is rather insensitive to flow [34]. Thus, not identified charged particles $\langle p_T \rangle$ may be considered as an estimation of the system temperature because it's not influenced very much by a possible transverse expansion. Furthermore, transverse radius $\mathrm{R_{side}}$ vs pair transverse momentum k_T in pp Bose Einstein correlation measures [24] show that, at least until $\frac{dN_{ch}}{d\eta} \simeq 3.4$, results are consistent with the

absence of transverse expansion, which further supports the adoption of $\langle p_T \rangle$ as an identifier of temperature, because it's little affected by the expansion.

Since a substantial number of pions is the product of resonance decay and the particles originating from the resonance decays populate the low p_T region [11], in this work we consider mainly $\langle p_T \rangle$ vs $\frac{dN_{ch}}{d\eta}$ correlations with a $p_{T\ \mathrm{min}}$ cut (> 400 MeV/c in CDF experiments Run I and Run II , > 500 MeV/c in ALICE, and two different cuts, > 500 MeV/c and > 2500 MeV/c, in ATLAS experiment) in order to work with $\langle p_T \rangle$ values less influenced by this effect. Furthermore, diffractive events are substantially reduced for $\frac{dN_{ch}}{d\eta} \gtrsim 2$ in $\langle p_T \rangle$ vs $\frac{dN_{ch}}{d\eta}$ plots with $p_{T\ \mathrm{min}} \geq 400$ MeV/c [21, 22].

We will show anyway also some results for $\langle p_T \rangle$ computed with $p_{T\ \mathrm{min}}$ cut 0 and > 100 MeV/c. The structure of the relations we are going to show is still present in these measures.

In this work, $\langle p_T \rangle$ computed for different p_T cuts will be plotted without the application of corrections due to the cut in the used p_T range, apart from the case of events energy density estimation, in which we will use a corrected $\langle p_T \rangle$. Regarding $\frac{dN_{ch}}{d\eta}$, it is computed from the number of particle in a given region of pseudorapidity η and p_T, dividing by the amplitude of the η range and properly correcting for p_T cuts. In order to perform this last correction, we considered $\frac{dN_{ch}}{d\eta}$ curves for the different experiments, measured with and without p_T cuts, and multiplied by the ratio between correspondent values of $\frac{dN_{ch}}{d\eta}$ in the central region. All data are obtained from minimum bias experiments. For CDF run II 1960 GeV, high multiplicity trigger data are added to minimum bias data, for charged particle multiplicity $N_{ch} \geq 22$ ($|\eta| < 1$, $p_T > 400$ MeV/c corresponding to $\frac{dN_{ch}}{d\eta}$ corrected ≥ 22) [15, 28].

Where available, we considered also raw data results (i.e. computed without experimental inefficiencies corrections) because the $\langle p_T \rangle$ vs $\frac{dN_{ch}}{d\eta}$ plot and its derived plots are much sensible to experimental losses and, on the other hand, the application of corrections may involve some "smearing" of data which could highly modify the analyzed effects [19, 35]. For reasons of space we don't show behaviors for raw data in this paper, because results are very similar to those for corrected data.

2.2. Entropy Density Estimation

The initial energy density in the rest system of a head-on collision has been argued to be [6]:

$$\epsilon \simeq \frac{\frac{dN_{ch}}{d\eta} \cdot \frac{3}{2} \langle p_T \rangle}{V}$$

V denotes the volume into which the energy is deposited. Similarly the initial entropy density is [2]:

$$\sigma \simeq \frac{\frac{dN_{ch}}{d\eta} \cdot \frac{3}{2}}{V}$$

As a result, ϵ is equal to $\sigma \cdot \langle p_T \rangle$. The volume V may be estimated as $V = S \cdot ct$, where S is the interaction area and ct is a longitudinal dimension we can traditionally consider to be about 1 fm long.

In order to study our system, we will use the quantity

$$\sigma_S = \frac{\frac{dN_{ch}}{d\eta} \cdot \frac{3}{2}}{S}$$

as an estimation of entropy density. In models like color glass condensate and percolation, the system physics depends on σ_S [36–38]. For the estimation of the area of interaction S, we proceed in different ways, our target being the obtainment of results which are robust respect to the definition of the area.

On the other hand, we are more interested in relations between variables than in their absolute values.

2.3. Bose Einstein correlation for emission region size estimation

Using Bose Einstein correlation among emitted particles, measurements of particle emission regions in many pp and $p\bar{p}$ experiments have been done [23–26, 31, 32, 39–41] In [23, 24], as already mentioned, the measurement of R_{side} in function of k_T in pp, shows that the transverse radius doesn't depend on k_T for low $\frac{dN_{ch}}{d\eta}$ values (< 3.4). This can be explained by the absence of expansion of the particle emission source, at least at these $\frac{dN_{ch}}{d\eta}$ values. For $\frac{dN_{ch}}{d\eta}$ values greater than 7, there is a dependence of R_{side} on k_T, so that probably a source expansion is possible at least from this $\frac{dN_{ch}}{d\eta}$ value. It is thus possible that a new phenomenon is started in events with $\frac{dN_{ch}}{d\eta}$ between 3.4 and 7. The hypothesis of no expansion for low $\frac{dN_{ch}}{d\eta}$ values lets us approximate the initial interaction section radius to be coincident to the final emission radius. We take into account that for $\frac{dN_{ch}}{d\eta}$ values greater than about 7.5, this approximation is more uncertain. Furthermore, resonance effects are present, but, once more, we are not interested in the absolute values of the interaction section, but in its behavior in function of $\frac{dN_{ch}}{d\eta}$. Not taking into account these effects yields a systematic error on the value of the radius, which we consider invariant for different values of $\frac{dN_{ch}}{d\eta}$. Given the similarity in both the behavior and the absolute values of R_{side} and invariant radius R_{inv} versus multiplicity, we use R_{inv} as an estimation of the interaction region radius, mainly because R_{inv} data where measured for a larger $\frac{dN_{ch}}{d\eta}$ range than R_{side} ones [23–26, 31, 32, 39, 40]. In Fig. 2, R_{inv} is shown as a function of pseudorapidity density. In the left we only show data for CMS (preliminary)

and ALICE (preliminary) at $\langle k_T \rangle \simeq 0.35$, while in the right side we show the same results along data from other experiments (UA1, ABCDHW ISR, STAR). We fitted the data of Fig. 2a with two functional relations between R_{inv} and $\frac{dN_{ch}}{d\eta}$: the first is linear in the cube root of $\frac{dN_{ch}}{d\eta}$ [23, 24, 42] and the second is linear in cube root of $\frac{dN_{ch}}{d\eta}$ for $\frac{dN_{ch}}{d\eta} > 7.5$, matched with a 5^{th} degree polynomial fit for smaller $\frac{dN_{ch}}{d\eta}$ values. The first fit gives a $\frac{\chi^2}{NDoF} = 0.84$ with p-value: 0.67, while the second gives a $\frac{\chi^2}{NDoF} = 0.45$ with p-value: 0.95. Considering these results, we opted to use the second fit for the following analysis.

It has been stated that the behavior of radii in function of $\frac{dN_{ch}}{d\eta}$ doesn't depend on the experiment energy [41]. Data in Fig. 2 seem to confirm this statement, and justify our choice of a single relation for R_{inv} vs $\frac{dN_{ch}}{d\eta}$ for all energies.

In order to estimate the interaction region, we used the following alternatives:

1. An area obtained using R_{inv} from the combined (polynomial + linear in cube root of $\frac{dN_{ch}}{d\eta}$) fit from Fig 2a. This choice may overestimate the interaction region in case of system expansion, being R_{inv} a measure of the emission region;
2. following ALICE results in R_{side} vs k_T, we make the hypothesis that no expansion is present in events with sufficiently low $\frac{dN_{ch}}{d\eta}$. So we use R_{inv} from the left (polynomial) part of the combined fit in Fig 2a, then we use a constant radius for $\frac{dN_{ch}}{d\eta} > 7.5$ as an estimation of the dimensions of the initial region before the possible expansion, making the assumption that at $\frac{dN_{ch}}{d\eta} \simeq 7.5$ the interaction region reaches its

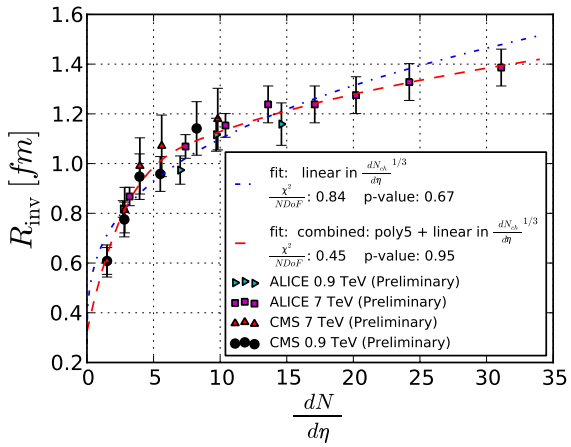

(a)

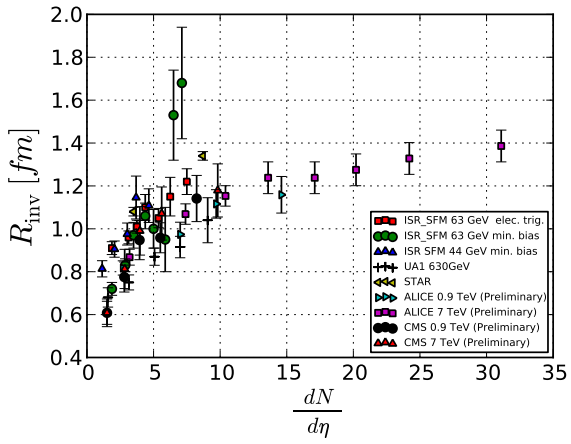

(b)

Figure 2: $R_{\rm inv}$ vs $\frac{dN_{ch}}{d\eta}$ for different experiments [23–26, 31, 32, 40]. Left plot shows data from CMS (preliminary) and ALICE(preliminary) both at $\langle k_T \rangle \simeq 0.35$, along with linear fit in $\frac{dN_{ch}}{d\eta}^{\frac{1}{3}}$ and a combined fit: $5^{\rm th}$ degree polynomial for $\frac{dN_{ch}}{d\eta} < 7.5$ matched to linear fit in $\frac{dN_{ch}}{d\eta}^{\frac{1}{3}}$ for $\frac{dN_{ch}}{d\eta} > 7.5$. Right plot shows data from the first plot along with data from UA1, ABCDHW ISR, and STAR experiments.

maximum; at $\frac{dN_{ch}}{d\eta} = 7.5$ the R_{inv} value is 1.08 fm;

3. an area obtained from a model which relates the impact parameter to the multiplicity of events [33].

From $\frac{dN_{ch}}{d\eta}$ values and from interaction areas, estimated as described above, we obtained the values of density of particles for transverse area.

We considered the simplified case where the central blob volume V is the same in all collisions for a given $\frac{dN_{ch}}{d\eta}$ [12]. We estimate an average σ from the ratio between $\frac{dN_{ch}}{d\eta}$ and the estimated average V.

2.4. $\sigma_S/\langle p_T\rangle^3$ *vs* $\langle p_T\rangle$

Using the estimated σ_S, the relation $\langle p_T\rangle$ vs σ_S can be studied. A slope change in $\langle p_T\rangle$ vs σ_S plots is found at σ_S between 2.5 and 3 fm^{-2}, depending on the method used for the estimation of area S and corresponds directly to the slope change seen in $\langle p_T\rangle$ vs $\frac{dN_{ch}}{d\eta}$ at $\frac{dN_{ch}}{d\eta} \simeq 6$.

Starting from σ_S and $\langle p_T\rangle$, we plotted $\sigma_S/\langle p_T\rangle^3$ vs $\langle p_T\rangle$ curves, as an experimental approximation of σ/T^3 vs T curves. See Figs. 3 and 4. We obtained very similar $\sigma_S/\langle p_T\rangle^3$ vs $\langle p_T\rangle$ curves from other pp and p$\bar{\text{p}}$ experiments [27, 29–31] (not shown).

In figures, we put labels with corresponding $\frac{dN_{ch}}{d\eta}$ values for interesting points, in order to relate these points to the characteristic values in $\frac{dN_{ch}}{d\eta}$. In the different plots, different regions are recognizable. In particular, in all plots we see that from the $\sigma_S/\langle p_T\rangle^3$ value corresponding to $\frac{dN_{ch}}{d\eta} \simeq 2$, up to a value correspondent to $\frac{dN_{ch}}{d\eta} \simeq 6$, the curve is almost flat, then rises very quickly. This behavior is similar to the one in σ/T^3 curve, in presence of crossover, starting from a state of matter, identified by σ/T^3 nearly constant

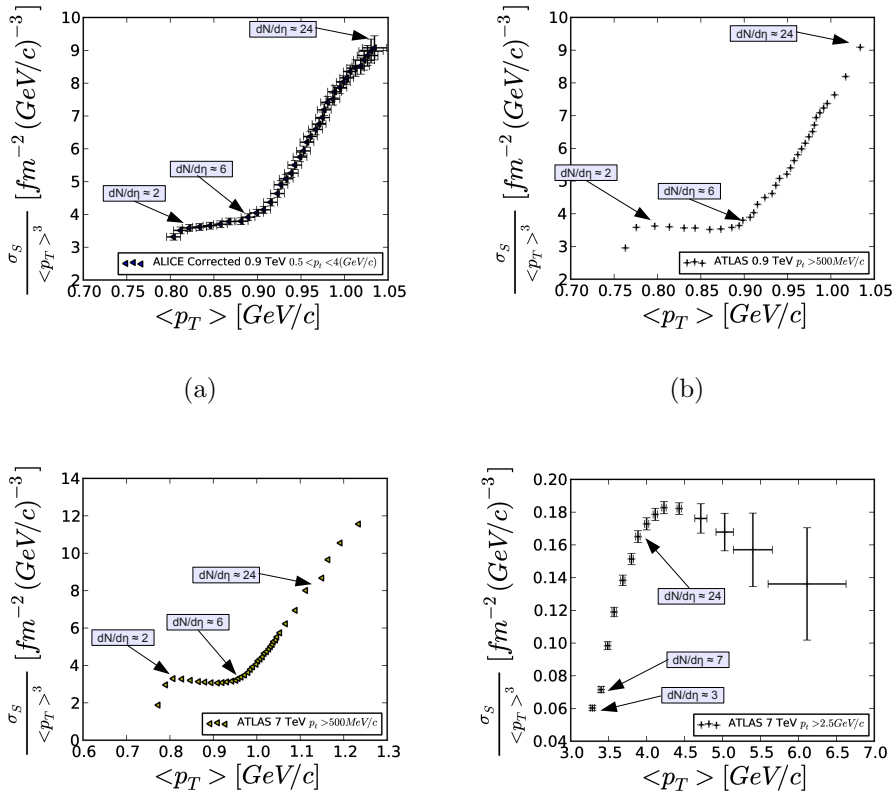

Figure 3: $\sigma_S/\langle p_T\rangle^3$ vs $\langle p_T\rangle$ plots. Area S from "5$^{\text{th}}$ degree polynomial + constant after $\frac{dN_{ch}}{d\eta} > 7.5$" fit.

3a: ALICE at $\sqrt{s} = 0.9$ TeV, $0.5 < p_T < 4$ GeV/c, $|\eta| < 0.8$, Minimum Bias.

3b: ATLAS at $\sqrt{s} = 0.9$ TeV, $p_T > 0.5$ GeV/c, $|\eta| < 2.5$, Minimum Bias.

3c: ATLAS at $\sqrt{s} = 7$ TeV, $p_T > 0.5$ GeV/c, $|\eta| < 2.5$, Minimum Bias.

3d: ATLAS at $\sqrt{s} = 7$ TeV, $p_T > 2.5$ GeV/c, $|\eta| < 2.5$, Minimum Bias.

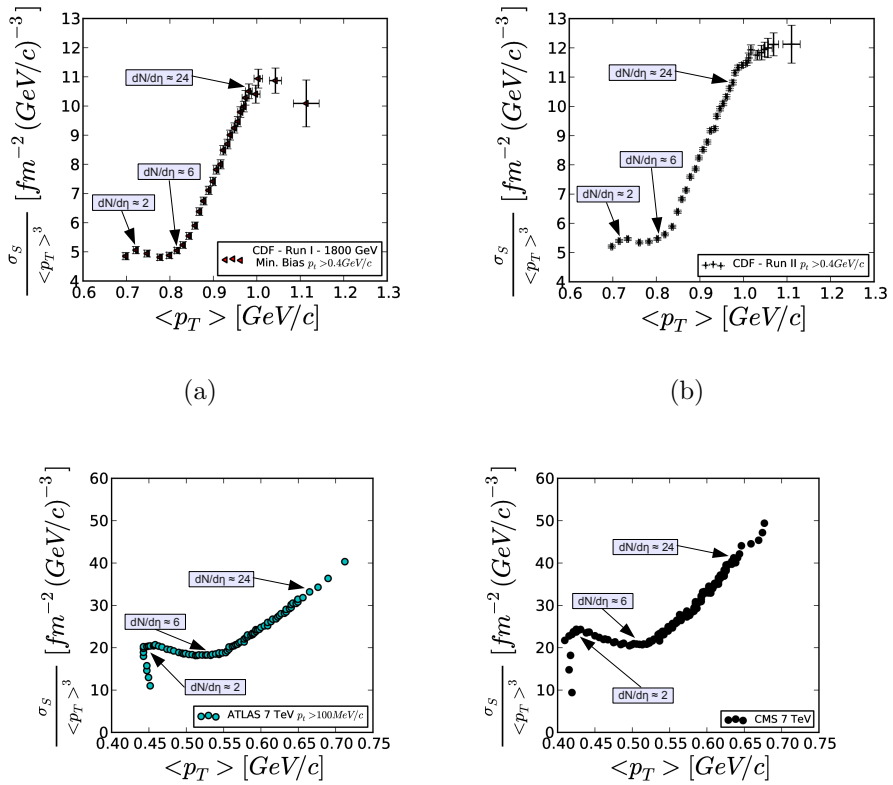

(a) (b)

(c) (d)

Figure 4: $\sigma_S/\langle p_T\rangle^3$ vs $\langle p_T\rangle$ plots. Area S from "5$^{\text{th}}$ degree polynomial + constant after $\frac{dN_{ch}}{d\eta} > 7.5$" fit.

4a: CDF Run I at $\sqrt{s} = 1.8$ TeV, $p_T > 0.4$ GeV/c, $|\eta| < 1.0$, Minimum Bias.

4b: CDF Run II at $\sqrt{s} = 1.96$ TeV, $p_T > 0.4$ GeV/c, $|\eta| < 1.0$, Minimum Bias + High multiplicity trigger.

4c: ATLAS at $\sqrt{s} = 7$ TeV, $p_T > 0.1$ GeV/c, $|\eta| < 2.5$, Minimum Bias.

4d: CMS at $\sqrt{s} = 7$ TeV, $p_T > 0$ GeV/c, $|\eta| < 2.4$. Minimum Bias.

(region $2 \lesssim \frac{dN_{ch}}{d\eta} \lesssim 6$), and a crossover starting at $\frac{dN_{ch}}{d\eta} \simeq 6$ (Fig. 1). Besides, in plots with many points at high $\frac{dN_{ch}}{d\eta}$ values (ATLAS with $p_T > 2500$ MeV/c, and CDF Run II 1960 GeV with $p_T > 400$ MeV), we observe a strong slope change around corresponding $\frac{dN_{ch}}{d\eta}$ values of about 24 or higher. It's worth noting that what seems to be a different behavior in the left side for ATLAS with $p_T > 2500$ MeV/c (Fig. 3d), is only due to the fact that all points correspond to $\frac{dN_{ch}}{d\eta} \gtrsim 7$, apart from the first point, which correspond to $\frac{dN_{ch}}{d\eta} \simeq 3.4$. The ratio between $\sigma_S/\langle p_T \rangle^3$ values corresponding to $\frac{dN_{ch}}{d\eta} \geq 24$ and those corresponding to $\frac{dN_{ch}}{d\eta} \leq 6$ varies from 2 to 3, depending on the area calculation method used for the estimation of σ_S. This ratio in the case of EOS would correspond to the ratio between the number of the degrees of freedom of the state before and after the transition or the crossover. We note that for small size systems as it would be in the pp case, the jump in entropy density is considerably reduced [8–10] in comparison to the theoretical infinite volume case. In plots with $p_T > 100$ MeV/c (ATLAS 7 TeV) or $p_T > 0$ (CMS 7 TeV), the first points have constant $\langle p_T \rangle$ with varying $\frac{dN_{ch}}{d\eta}$, which leads to an initial steep rise. After that, the curves assume the same behavior of previously seen plots.

2.5. Sound velocity c_s^2

One of the physical quantities used to characterize the state of a system is its squared sound velocity, defined as $c_s^2 = \frac{\sigma}{T} \cdot \frac{dT}{d\sigma}$, for constant V [11]. In our study, we approximate it with $c_s^2 = \frac{\sigma_S}{\langle p_T \rangle} \cdot \frac{d\langle p_T \rangle}{d\sigma_S}$. It is really interesting that if $\langle p_T \rangle$ is proportional to T and if σ_S is proportional to the entropy density, then the c_s^2 value obtained in this approximation is equal to the right value

of $c_s^2 = \frac{\sigma}{T} \cdot \frac{dT}{d\sigma}$, because proportionality constants cancel out. In order to obtain our c_s^2 estimation, from $\langle p_T \rangle$ vs $\frac{dN_{ch}}{d\eta}$ curves and from σ_S values, we compute the curve $\langle p_T \rangle$ vs σ_S, to which we apply numerical derivation. We cope with the statistical fluctuation in data points using a combination of Gaussian and Savitzky-Golay filters [43]. Examples of c_s^2 vs $\langle p_T \rangle$ curves are shown in Figs. 5a and 5c.

The so obtained c_s^2 estimation resembles the typical shape of a phase transition or a crossover: a descent, a minimum region and a following rise, as it's also obtained analytically from EOSs which present a phase transition or a crossover. The minimum value reached by the estimation of c_s^2 in the different experimental curves varies from 0.08 to 0.18 and could correspond to what it's called the EOS softest point [17].

Recently Refs. [44–46] estimate c_s^2 minimum value for realistic EOS to be around 0.14. From $\epsilon_S \simeq \langle p_T \rangle \cdot \sigma_S$ we compute c_s^2 vs ϵ_S curves, that are approximations of c_s^2 vs energy density. We report these curves in Figs. 5b and 5d.

In this case, ϵ_S values are calculated using $\langle p_T \rangle$ values from $\langle p_T \rangle$ vs $\frac{dN_{ch}}{d\eta}$ curves with no $p_{T\ \mathrm{min}}$ cut at corresponding energies, estimated in correspondence with the different $\frac{dN_{ch}}{d\eta}$ values. As Figs. 5 show, the numerical estimation of c_s^2 vs ϵ_S, is characterized by a maximum at low energy density followed by a minimum region, which is obtained for ϵ_S values in range $1.5 - 2.0$ GeV/fm^2, and a subsequent rise.

We note that ϵ_S as computed here is an estimation of the energy density for pseudorapidity unit and unit of transverse area. In order to estimate the volume energy density this should be divided by ct.

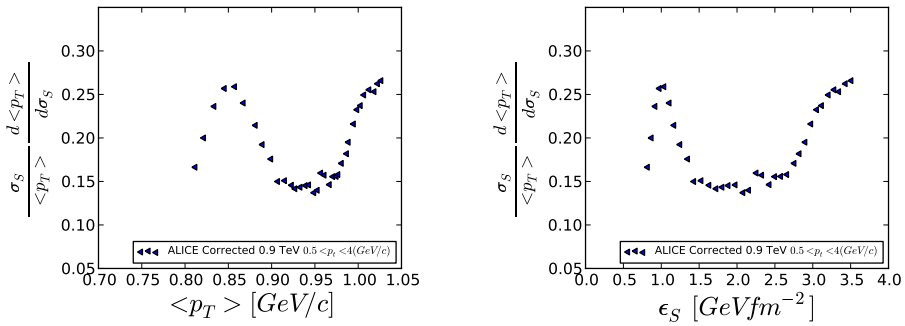

(a)

(b)

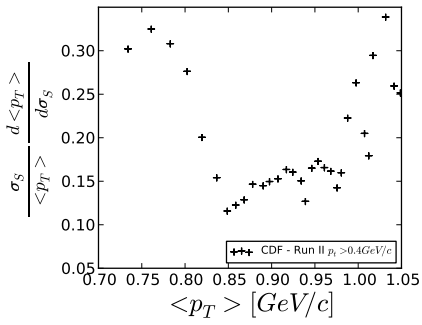

(c)

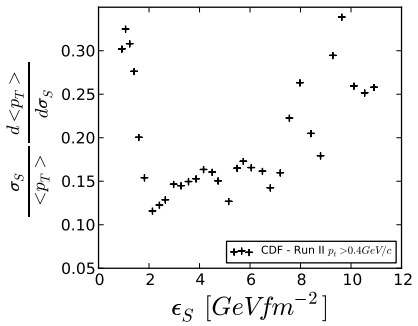

(d)

Figure 5: $c_s^2 = \dfrac{\sigma_S}{\langle p_T \rangle} \cdot \dfrac{d\langle p_T \rangle}{d\sigma_S}$ vs $\langle p_T \rangle$ or ϵ_S, using two different fits for area S estimation.

ALICE at $\sqrt{s} = 0.9$ TeV, $0.5 < p_T < 4$ GeV/c, $|\eta| < 0.8$, Minimum Bias; area S from "5$^{\text{th}}$ degree polynomial + linear in $\frac{dN_{ch}}{d\eta}^{1/3}$ after $\frac{dN_{ch}}{d\eta} > 7.5$" fit.

5a: c_s^2 vs $\langle p_T \rangle$, 5b: c_s^2 vs ϵ_S.

CDF Run II at $\sqrt{s} = 1.96$ TeV, $p_T > 0.4$ GeV/c, $|\eta| < 1.0$, Minimum Bias + High multiplicity trigger; area S from "5$^{\text{th}}$ degree polynomial + constant after $\frac{dN_{ch}}{d\eta} > 7.5$" fit.

5c: c_s^2 vs $\langle p_T \rangle$, 5d: c_s^2 vs ϵ_S.

3. Discussion

The shape of the $\sigma_S/\langle p_T\rangle^3$ approximation to the EOS is very similar, using both R_{inv} from the fit on all $\frac{dN_{ch}}{d\eta}$ space and R_{inv} fitted up to $\frac{dN_{ch}}{d\eta} = 7.5$ and then maintained constant. It slightly varies when using the area from the impact parameter model, but the slope change at $\sigma_S/\langle p_T\rangle^3$ values corresponding to $\frac{dN_{ch}}{d\eta}$ around 6 is still present, as well as the change at $\sigma_S/\langle p_T\rangle^3$ values corresponding to $\frac{dN_{ch}}{d\eta}$ about 24.

In order to avoid possible systematics due to calculation involved in the area definition, we plotted directly $\frac{dN_{ch}}{d\eta}/\langle p_T\rangle^3$ vs $\langle p_T\rangle$: this is equivalent to obtain $\sigma_S/\langle p_T\rangle^3$ curves considering a transverse section which is constant for all $\frac{dN_{ch}}{d\eta}$ values. For space reason we don't show these plots in this paper. In this case the shape doesn't resemble an EOS shape anymore, but the slope changes at $\frac{dN_{ch}}{d\eta} \simeq 6$ and $\frac{dN_{ch}}{d\eta} \simeq 24$ are still present, because they are contained in the $\langle p_T\rangle$ vs $\frac{dN_{ch}}{d\eta}$ correlation.

The shape of the curves obtained from experimental data ($\sigma_S/\langle p_T\rangle^3$ vs $\langle p_T\rangle$, c_s^2 vs $\langle p_T\rangle$ and c_s^2 vs energy) depends on experimental $\langle p_T\rangle$ vs $\frac{dN_{ch}}{d\eta}$ curves and from the value of the area used to obtain density sigmas. Systematic errors in $\langle p_T\rangle$, $\frac{dN_{ch}}{d\eta}$, and R_{inv} measurements don't lead to appreciable variations in $\langle p_T\rangle$ vs σ_S behavior, which is what we are interested on.

It seems to us that the main result of this work is that putting together experimental data of $\langle p_T\rangle$ vs $\frac{dN_{ch}}{d\eta}$ and R_{inv} vs $\frac{dN_{ch}}{d\eta}$, curves are obtained which are the reproduction of theoretical EOS curves.

Regarding model comparison, we obtained $\sigma_S/\langle p_T\rangle^3$ vs $\langle p_T\rangle$ plots starting from Montecarlo curves (*Pythia ATLAS AMBT1* and *Pythia8* for ATLAS and CMS experiment respectively), which are shown in Fig. 6.

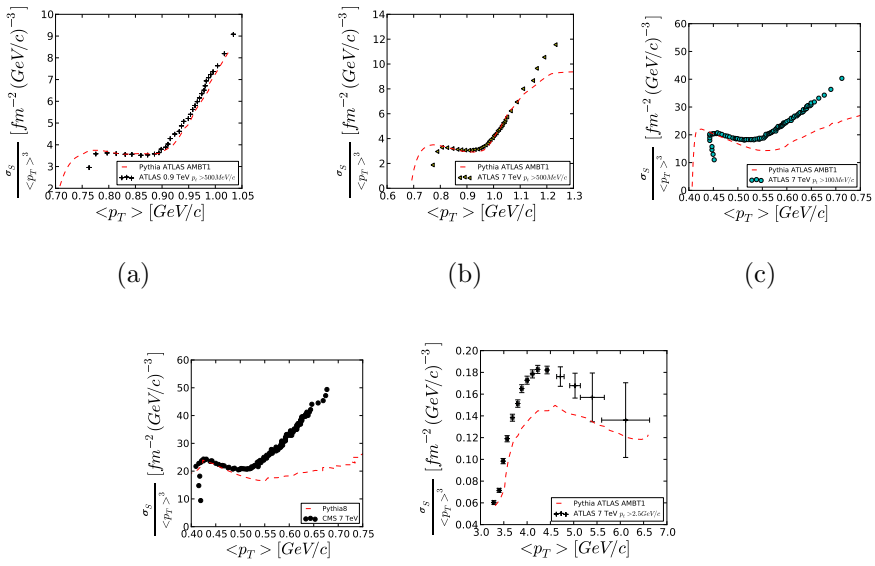

Figure 6: $\sigma_S/\langle p_T\rangle^3$ vs $\langle p_T\rangle$. Comparison with models.

6a: ATLAS at $\sqrt{s} = 0.9$ TeV, $p_T > 0.5$ GeV/c, $|\eta| < 2.5$, Minimum Bias and *Pythia ATLAS AMBT1*.

6b: ATLAS at $\sqrt{s} = 7$ TeV, $p_T > 0.5$ GeV/c, $|\eta| < 2.5$, Minimum Bias and *Pythia ATLAS AMBT1*.

6c: ATLAS at $\sqrt{s} = 7$ TeV, $p_T > 0.1$ GeV/c, $|\eta| < 2.5$, Minimum Bias and *Pythia ATLAS AMBT1*.

6d: CMS at $\sqrt{s} = 7$ TeV, $p_T > 0$ GeV/c, $|\eta| < 2.4$, Minimum Bias and *Pythia8*.

6e: ATLAS at $\sqrt{s} = 7$ TeV, $p_T > 2.5$ GeV/c, $|\eta| < 2.5$, Minimum Bias and *Pythia ATLAS AMBT1*.

Some models on which tuning has been done, for example with CDF Run II data at 1960 GeV for $p_T > 400$ MeV/c, well reproduce the $\langle p_T \rangle$ vs $\frac{dN_{ch}}{d\eta}$ curve at higher (7 TeV) or lower (0.9 TeV) energies with $p_T > 500$MeV/c. It is clear that in these cases, starting from the $\langle p_T \rangle$ vs $\frac{dN_{ch}}{d\eta}$ curves of models and using Bose Einstein correlation or the impact parameter–multiplicity relation for σ_S estimation, curves similar to the experimental ones are obtained. On the other hand, models don't predict well $\langle p_T \rangle$ vs $\frac{dN_{ch}}{d\eta}$ curves with low $p_{T\ \mathrm{min}}$, and consequently $\sigma_S/\langle p_T \rangle^3$ vs $\langle p_T \rangle$ curves as shown for the comparison of models at 7 TeV for CMS and ATLAS data, respectively with $p_T > 0$ MeV/c and $p_T > 100$ MeV/c [20–22, 47].

The interpretation of curve shapes as experimental "estimation" of EOS depends on how much likely are the correspondences between $\langle p_T \rangle$ and T, and between measured σ_S and entropy.

4. Conclusion

The result we consider to be the most important is the following: in many experiments [19–22, 27–31] from 31 GeV to 7000 GeV, starting from $\langle p_T \rangle$ vs $\frac{dN_{ch}}{d\eta}$ and using results from measures of radii with Bose Einstein correlation or from a model that relates impact parameter and multiplicity, we obtained that $\sigma_S/\langle p_T \rangle^3$ vs $\langle p_T \rangle$ and $\mathrm{c_s^2} = \dfrac{\sigma_S}{\langle p_T \rangle} \cdot \dfrac{d\langle p_T \rangle}{d\sigma_S}$ reproduce the shape of hadronic matter EOSs and squared sound velocity respectively, in presence of crossover or phase transition. From the plots, a neat change around $\frac{dN_{ch}}{d\eta}$ around 6, where the crossover or the phase transition seems to start, and another possible change at $\frac{dN_{ch}}{d\eta}$ around 24 are observed. The curve $\mathrm{c_s^2}$ vs ϵ_S has a minimum around a "transverse" energy density of about 1.5 GeV/fm^2.

In order to understand if these behaviors have a real physical meaning or are just casual, results of measures in the following regions should be compared: $2 \lesssim \frac{dN_{ch}}{d\eta} \lesssim 6$, $\frac{dN_{ch}}{d\eta} \gtrsim 6$, $6 \lesssim \frac{dN_{ch}}{d\eta} \lesssim 24$ and $\frac{dN_{ch}}{d\eta} \gtrsim 24$.

References

References

[1] Y. Aoki, G. Endrodi, Z. Fodor, S. D. Katz, K. K. Szabó, The order of the quantum chromodynamics transition predicted by the standard model of particle physics., Nature 443 (2006) 675–8.

[2] K. Redlich, H. Satz, Critical behavior near deconfinement, Physical Review D 33 (1986) 3747.

[3] P. Braun-Munzinger, J. Stachel, The quest for the quark-gluon plasma., Nature 448 (2007) 302–9.

[4] L. C. P. Van Hove, Two problems concerning hot hadronic matter and high energy collisions (equilibrium formation, plasma deflagration), Z. Phys. C Particles and Fields 21 (1983) 93–98.

[5] K. Werner, I. Karpenko, T. Pierog, "Ridge" in Proton-Proton Scattering at 7 TeV, Physical Review Letters 106 (2011).

[6] J. D. Bjorken, Highly relativistic nucleus-nucleus collisions: The central rapidity region, Physical Review D 27 (1983) 140–151.

[7] P. Castorina, D. Kharzeev, H. Satz, Thermal hadronization and Hawking–Unruh radiation in QCD, The European Physical Journal C 52 (2007) 187–201.

[8] H.-T. Elze, W. Greiner, Finite size effects for quark-gluon plasma droplets, Physics Letters B 179 (1986) 385–392.

[9] A. Bazavov, B. Berg, Deconfining phase transition on lattices with boundaries at low temperature, Physical Review D 76 (2007) 014502.

[10] L. F. Palhares, E. S. Fraga, T. Kodama, Finite-size effects and signatures of the QCD critical endpoint, Journal of Physics G: Nuclear and Particle Physics 37 (2010) 094031.

[11] W. Florkowski, Phenomenology of Ultra-relativistic Heavy-ion Collisions, World Scientific Publishing Company, 2010.

[12] L. Van Hove, Multiplicity dependence of pt spectrum as a possible signal for a phase transition in hadronic collisions, Physics Letters B 118 (1982) 138–140.

[13] B. Muller, Physics and signatures of the quark-gluon plasma, Reports on Progress in Physics 58 (1995) 611–636.

[14] B. Mohanty, J. Alam, S. Sarkar, T. K. Nayak, B. K. Nandi, Indication of a coexisting phase of quarks and hadrons in nucleus-nucleus collisions, Physical Review C 68 (2003).

[15] R. Campanini, Possible Signals of new phenomena in hadronic interactions at dn/deta=5.5+-1.2, Arxiv preprint arXiv:1102.5219v1 [hep-ex] (2010) 32.

[16] R. Campanini, Quark gluon plasma and multiplicity dependence of

transverse momentum in hadronic collisions, Lettere Al Nuovo Cimento Series 2 44 (1985) 343–350.

[17] E. Shuryak, Is the explosion of a quark-gluon plasma found?, Physics Letters B 171 (1986) 99–102.

[18] T. Alexopoulos, E. Anderson, A. Bujak, D. Carmony, A. Erwin, L. Gutay, A. Hirsch, K. Nelson, N. Porile, S. Oh, Evidence for hadronic deconfinement in collisions at 1.8 TeV, Physics Letters B 528 (2002) 43–48.

[19] K. Aamodt, N. Abel, U. Abeysekara, A. Abrahantes Quintana, A. Abramyan, D. Adamová, M. Aggarwal, G. Aglieri Rinella, A. Agocs, S. Aguilar Salazar, Transverse momentum spectra of charged particles in proton–proton collisions at $\sqrt{s} = 900$ GeV with ALICE at the LHC, Physics Letters B 693 (2010) 53–68.

[20] V. Khachatryan, A. M. Sirunyan, A. Tumasyan, W. Adam, T. Bergauer, M. Dragicevic, J. Erö, F. et al., Charged particle multiplicities in pp interactions at $\sqrt{s} = 0.9$, 2.36, and 7 TeV, Journal of High Energy Physics 2011 (2011).

[21] G. Aad, E. Abat, B. Abbott, J. Abdallah, A. Abdelalim, A. Abdesselam, O. Abdinov, B. e. Abi, Charged-particle multiplicities in pp interactions at $\sqrt{s} = 900$ GeV measured with the ATLAS detector at the LHC, Physics Letters B 688 (2010) 21–42.

[22] G. Aad, B. Abbott, J. Abdallah, A. A. Abdelalim, A. Abdesselam, O. Abdinov, B. Abi, M. Abolins, A. et al., Charged-particle multi-

plicities in pp interactions measured with the ATLAS detector at the LHC, New Journal of Physics 13 (2011) 053033.

[23] K. Aamodt, N. Abel, U. Abeysekara, A. Abrahantes Quintana, A. Abramyan, D. Adamová, M. Aggarwal, G. A. et al., Two-pion Bose-Einstein correlations in pp collisions at $\sqrt{s} = 900$ GeV, Physical Review D 82 (2010) 1–14.

[24] ALICE Collaboration, Femtoscopy of pp collisions at $\sqrt{s} = 0.9$ and 7 TeV at the LHC with two-pion Bose-Einstein correlations, Arxiv preprint arXiv:1101.3665 [hep-ex] (2011) 21.

[25] V. Khachatryan, A. Sirunyan, A. Tumasyan, W. Adam, T. Bergauer, M. Dragicevic, J. Erö, F. et al., First Measurement of Bose-Einstein Correlations in Proton-Proton Collisions at $\sqrt{s} = 0.9$ and 2.36 TeV at the LHC, Physical Review Letters 105 (2010) 1–14.

[26] The CMS Collaboration, Measurement of Bose-Einstein Correlations in pp Collisions at $\sqrt{s} = 0.9$ and 7 TeV, Arxiv preprint arXiv:1101.3518v1 [hep-ex] (2011).

[27] D. Acosta, T. Affolder, H. Akimoto, M. Albrow, P. Amaral, D. Ambrose, D. Amidei, K. A. et al., Soft and hard interactions in pp^- collisions at $\sqrt{s} = 1800$ and 630 GeV, Physical Review D 65 (2002).

[28] T. Aaltonen, J. Adelman, T. Akimoto, B. González, S. Amerio, D. Amidei, A. Anastassov, A. A. et al., Measurement of particle production and inclusive differential cross sections in pp^- collisions at $\sqrt{s} = 1.96$ TeV, Physical Review D 79 (2009).

[29] T. Alexopoulos, C. Allen, E. W. Anderson, V. Balamurali, S. Banerjee, P. D. Beery, P. Bhat, J. M. B. et al., Mass-identified particle production in proton-antiproton collisions at $\sqrt{s}$ = 300, 540, 1000, and 1800 GeV, Physical Review D 48 (1993) 984–997.

[30] C. Albajar, A study of the general characteristics of proton-antiproton collisions at $\sqrt{s}$ = 0.2 to 0.9 TeV, Nuclear Physics B 335 (1990) 261–287.

[31] A. Breakstone, R. Campanini, H. B. Crawley, M. Cuffiani, G. M. Dallavalle, M. M. Deninno, K. Doroba, D. D. et al., Multiplicity dependence of the average transverse momentum and of the particle source size in p–p interactions at $\sqrt{s}$ = 62, 44 and 31 GeV, Zeitschrift für Physik C Particles and Fields 33 (1987) 333–338.

[32] STAR Collaboration, Pion femtoscopy in p+p collisions at sqrt(s)=200 GeV, Arxiv preprint arXiv:1004.0925v2 [nucl-ex] (2010) 16.

[33] A. Bialas, E. Bialas, Impact parameter analysis of multiplicity distribution in high-energy p p collisions, Acta Physica Polonica B 5 (1974) 373.

[34] E. V. Shuryak, QCD Vacuum, Hadrons and Superdense Matter, World Scientific Publishing Company, Singapore, 2nd revised edition, 2003.

[35] N. Moggi, Soft Multiparticle Production in p^- p Interactions at 1800 and 630 GeV, Phd. thesis, University of Pavia, 1999. Available at `www-cdf.fnal.gov/thesis/cdf5329_soft_multiparticle.ps.gz`.

[36] L. McLerran, R. Venugopalan, Computing quark and gluon distribution functions for very large nuclei, Physical Review D 49 (1994) 2233–2241.

[37] J. Dias De Deus, C. Pajares, Percolation of color sources and critical temperature, Physics Letters B 642 (2006) 455–458.

[38] H. Satz, Colour deconfinement in nuclear collisions, Reports on Progress in Physics 63 (2000) 1511–1574.

[39] T. Alexopoulos, C. Allen, E. Anderson, V. Balamurali, S. Banerjee, P. Beery, P. Bhat, J. B. et al., Study of source size in pp^- collisions at $\sqrt{s} = 1.8$ TeV using pion interferometry, Physical Review D 48 (1993) 1931–1942.

[40] C. Albajar, Bose-Einstein correlations in p interactions at $\sqrt{s} = 0.2$ to 0.9 TeV, Physics Letters B 226 (1989) 410–416.

[41] Z. Chajęcki, Femtoscopy in hadron and lepton collisions: RHIC results and world systematics, Acta Physica Polonica B 40 (2009) 1119–1136.

[42] M. A. Lisa, S. Pratt, Femtoscopically Probing the Freeze-out Configuration in Heavy Ion Collisions (ed.), in: R. Stock (Ed.), SpringerMaterials - The Landolt-Börnstein Database – `http://www.springermaterials.com`, Springer-Verlag, Berlin Heidelberg, 2010, pp. 1–33.

[43] A. Savitzky, M. J. E. Golay, Smoothing and Differentiation of Data by Simplified Least Squares Procedures., Analytical Chemistry 36 (1964) 1627–1639.

[44] P. Castorina, J. Cleymans, D. E. Miller, H. Satz, The speed of sound in hadronic matter, The European Physical Journal C 66 (2010) 207–213.

[45] B. K. Srivastava, Percolation and Deconfinement, Arxiv preprint arXiv:1102.0754v1 [nucl-ex] (2011) 1–8.

[46] M. Chojnacki, W. Florkowski, Temperature dependence of sound velocity and hydrodynamics of ultra-relativistic heavy-ion collisions, Acta Physica Polonica B 38 (2007) 3249–3262.

[47] CMS Collaboration, Charged particle multiplicities in pp interactions at $\sqrt{s} = 0.9$, 2.36, and 7 TeV, Arxiv preprint arXiv:1011.5531v1 (2010).